



This is a repository copy of *Polydimethylsiloxane-Based Diblock Copolymer Nano-objects Prepared in Nonpolar Media via RAFT-Mediated Polymerization-Induced Self-Assembly*.

White Rose Research Online URL for this paper:  
<http://eprints.whiterose.ac.uk/95174/>

Version: Accepted Version

---

**Article:**

Lopez-Oliva, A.P., Warren, N.J., Rajkumar, A. et al. (5 more authors) (2015)  
*Polydimethylsiloxane-Based Diblock Copolymer Nano-objects Prepared in Nonpolar Media via RAFT-Mediated Polymerization-Induced Self-Assembly*. *Macromolecules*, 48 (11). pp. 3547-3555. ISSN 0024-9297

<https://doi.org/10.1021/acs.macromol.5b00576>

---

**Reuse**

Unless indicated otherwise, fulltext items are protected by copyright with all rights reserved. The copyright exception in section 29 of the Copyright, Designs and Patents Act 1988 allows the making of a single copy solely for the purpose of non-commercial research or private study within the limits of fair dealing. The publisher or other rights-holder may allow further reproduction and re-use of this version - refer to the White Rose Research Online record for this item. Where records identify the publisher as the copyright holder, users can verify any specific terms of use on the publisher's website.

**Takedown**

If you consider content in White Rose Research Online to be in breach of UK law, please notify us by emailing [eprints@whiterose.ac.uk](mailto:eprints@whiterose.ac.uk) including the URL of the record and the reason for the withdrawal request.



[eprints@whiterose.ac.uk](mailto:eprints@whiterose.ac.uk)  
<https://eprints.whiterose.ac.uk/>

# Polydimethylsiloxane-based Diblock Copolymer Nano-objects Prepared in Non-polar Media

## via RAFT-mediated Polymerization-Induced Self-Assembly

Alejandra P. Lopez-Oliva, Nicholas J. Warren\*, Arthi Rajkumar, Oleksandr O. Mykhaylyk,  
Matthew J. Derry, Kay Doncom, Matthew J. Rymaruk and Steven P. Armes\*

*Dainton Building, Department of Chemistry, The University of Sheffield,  
Brook Hill, Sheffield, Yorkshire, S3 7HF, UK*

**Abstract.** Monocarbinol-functionalized polydimethylsiloxane (PDMS; mean degree of polymerization = 66) was converted into a chain transfer agent (CTA) for reversible addition-fragmentation chain transfer (RAFT) polymerization via esterification. The degree of esterification was determined to be  $94 \pm 1 \%$  by  $^1\text{H}$  NMR spectroscopy and  $92 \pm 1 \%$  by UV absorption spectroscopy. This PDMS CTA was then utilized for the dispersion polymerization of benzyl methacrylate (BzMA) in *n*-heptane at  $70^\circ\text{C}$ . As the PBzMA block grows, it becomes insoluble in the reaction medium, which drives the *in situ* formation of PDMS-PBzMA diblock copolymer nanoparticles via polymerization-induced self-assembly (PISA). Depending on the precise reaction conditions, the final diblock copolymer chains can self-assemble to form spheres, worms or vesicles. Systematic variation of the copolymer concentration and the target degree of polymerization (DP) of the PBzMA block enables construction of a phase diagram that allows the reproducible targeting of pure copolymer morphologies, as judged by transmission electron microscopy and dynamic light scattering studies.  $^1\text{H}$  NMR spectroscopy studies confirm that relatively high BzMA conversions ( $> 90 \%$ ) can be achieved within 8 h at  $70^\circ\text{C}$ . Gel permeation chromatography studies (THF eluent) indicate high blocking efficiencies and relatively low final polydispersities ( $M_w/M_n = 1.14 - 1.34$ ). Small-angle X-ray scattering (SAXS) has been used to characterize selected examples of the spherical nanoparticles in order to obtain volume-average diameters, which increase monotonically when targeting longer DPs for the core-forming PBzMA block. A relatively high copolymer concentration ( $> 25 \%$  w/v) is required to obtain a pure worm phase, which occupies an extremely narrow region within the phase diagram. Selected worm and vesicle dispersions were also analyzed by SAXS, which enables determination of the mean worm cross-section, mean worm length and vesicle membrane thickness, respectively. In addition, the highly anisotropic worms formed free-standing gels in *n*-heptane, with rheology measurements indicating viscoelastic behavior and a gel storage modulus of around  $10^4$  Pa.

\* Author to whom correspondence should be addressed (s.p.ames@sheffield.ac.uk)

## Introduction

Polydimethylsiloxane (PDMS) is a highly hydrophobic polymer that exists as a liquid at room temperature.<sup>1</sup> It has a highly flexible backbone as a result of free rotation around its Si-O bonds, which leads to a relatively low glass transition temperature.<sup>2</sup> PDMS confers exceptional lubricity, which has led to its widespread use in many cosmetic formulations, despite its relatively high cost.<sup>3-7</sup> PDMS is typically prepared via anionic ring-opening polymerization of cyclic monomers such as D3 or D4.<sup>8,9</sup> This leads to good molecular weight control, but back-biting can become problematic at high monomer conversions.<sup>10-13</sup>

Controlled-structure PDMS-based materials have various applications in polymer and colloid science.<sup>2,14</sup> For example, monomethacrylate-capped PDMS macromonomers have been utilized as reactive steric stabilizers for the preparation of PDMS-stabilized latexes in supercritical CO<sub>2</sub>.<sup>15,16</sup> Similarly, there are several reports of PDMS-based macromonomers being used to stabilize the non-aqueous dispersion polymerization of methyl methacrylate.<sup>17-20</sup> Various PDMS-based diblock copolymers have also been explored in this context. For example, Dawkins and co-workers found that PDMS-polystyrene (PDMS-PS) diblock copolymers are effective stabilizers for poly(methyl methacrylate) (PMMA) particles prepared in *n*-alkanes, cyclohexane and Freon.<sup>21</sup> Deslandes et al. also reported the synthesis of similar diblock copolymers via anionic polymerization of styrene, followed by sequential addition of D3.<sup>22</sup> Amphiphilic PDMS-based diblock copolymers have also been prepared via anionic polymerization of hydrophilic monomers such as 2-(dimethylamino)ethyl methacrylate (DMA) in THF at 25-50°C from a monocarbinol (or bicarbinol) PDMS precursor.<sup>23,24</sup>

PDMS homopolymer has also been used in soft lithography, offering good-quality etch contrast because of its high silicon content.<sup>25</sup> However, much of the current focus of microelectronics research is in the field of block copolymer lithography. Here the desired nano-patterns are generated during bulk self-assembly, with the precise block composition dictating the copolymer morphology.<sup>26</sup> In this context, PDMS-PS diblock copolymers have been used to form defect-free trenches of controlled width and orientation.<sup>26</sup> Spheres, cylinders, hexagons or double-gyroid nanostructures can be obtained by varying the processing conditions.<sup>27,28</sup> In particular, there is growing interest in PDMS-based diblock copolymers that form cylindrical morphologies in the solid state, since selective pulsed plasma etching of the PDMS block can produce nanoscale silica lines.<sup>32-35</sup>

There are numerous literature reports of spherical micelles or vesicles with PDMS as the *core-forming or membrane-forming* block.<sup>29-31</sup> However, as far as we are aware, there are very few

studies that describe the preparation of colloiddally stable dispersions of diblock copolymer nano-objects (particularly worms/cylinders or vesicles) for which PDMS acts as a *stabilizer* block. Exceptionally, Iyama and Nose<sup>36</sup> prepared meta-stable spheres, worms/cylinders or vesicles using a *single* PDMS-polystyrene diblock copolymer in a dilute solvent mixture comprising *n*-octane and methylcyclohexane. We are also aware of several papers by Manners and Winnik describing the preparation of PDMS-stabilized rods in *n*-alkanes from diblock copolymers containing a crystallizable core-forming block.<sup>37,38</sup>

Living radical polymerization techniques such as atom transfer radical polymerization (ATRP)<sup>39,40</sup> or reversible addition-fragmentation chain transfer (RAFT) polymerization<sup>41,42</sup> have revolutionized synthetic polymer chemistry over the last two decades. Functional monomers can be readily polymerized with excellent control over target molecular weights and molecular weight distributions using relatively undemanding synthetic protocols.<sup>43</sup> Of particular relevance to the present work, PDMS has been employed both as a macro-initiator for ATRP syntheses and also as a macromolecular chain transfer agent (macro-CTA) for RAFT syntheses.<sup>44,45</sup> More specifically, Haddleton's group reported the synthesis of PDMS-based diblock and triblock copolymers via ATRP using either methyl methacrylate or 2-(dimethylamino)ethyl methacrylate. In the latter case, micellization in aqueous solution was studied using pyrene fluorescence and the copolymers exhibited similar critical micelle concentrations to those reported for commercial surfactants.<sup>44</sup> More recently, Perrier and co-workers described the attempted preparation of PDMS-poly(2-(dimethylamino)ethyl acrylate) diblock copolymers via RAFT polymerization in toluene.<sup>45</sup> However, subsequent self-assembly in aqueous solution led to partial *in situ* hydrolysis of the 2-(dimethylamino)ethyl acrylate residues to produce acrylic acid residues, and hence a statistical acrylic block comprising amine and acid functionality.

Over the last five years or so, polymerization-induced self-assembly (PISA) has become established as a highly versatile approach for the efficient synthesis of diblock copolymer nanoparticles in various media.<sup>46</sup> Dispersion polymerization formulations have been conducted in water,<sup>47-51</sup> lower alcohols<sup>52-57</sup> or *n*-alkanes<sup>46,58,59</sup> and in each case either spheres, worms or vesicles can be obtained as pure phases at relatively high solids. In this approach, reversible addition-fragmentation chain transfer (RAFT) polymerization<sup>60</sup> is utilized to generate the insoluble core-forming block, with the soluble precursor block being selected to confer steric stabilization in the solvent of interest. For example, a water-soluble polymer such as poly(glycerol monomethacrylate) can be selected for aqueous dispersion polymerization formulations,<sup>50,61,62</sup> whereas a highly hydrophobic poly(lauryl methacrylate) block is well-suited for PISA syntheses conducted in *n*-alkanes.<sup>46,59,63 64,65</sup>

In the present study, we have evaluated a PDMS chain transfer agent (CTA) as the steric stabilizer block for the preparation of PDMS-based diblock copolymer nano-objects in a non-polar solvent (*n*-heptane). The core-forming block was selected to be poly(benzyl methacrylate) (PBzMA), which is insoluble in *n*-heptane – this is a prerequisite for *in situ* self-assembly of the copolymer chains. Suitable conditions are established to obtain colloiddally stable diblock copolymer nanoparticles and synthesis parameters such as the target degree of polymerization of the PBzMA block and the copolymer concentration are systematically varied in order to tune the copolymer morphology. These diblock copolymers are characterized using a wide range of techniques, including gel permeation chromatography (GPC), proton nuclear magnetic resonance spectroscopy (<sup>1</sup>H NMR), visible absorption spectroscopy, dynamic light scattering (DLS), transmission electron microscopy (TEM), small-angle X-ray scattering (SAXS) and rheology.

## Experimental

**Materials.** Monocarbinol-terminated PDMS<sub>66</sub> (its mean degree of polymerization of 66 was determined by <sup>1</sup>H NMR spectroscopy by comparing the integrated signal of the two terminal oxymethylene protons with that of the dimethyl backbone protons) was purchased from Gelest (USA). Benzyl methacrylate (BzMA), *N,N'*-dicyclohexylcarbodiimide (DCC), 4-dimethylaminopyridine (DMAP), 2,2'-azobisisobutyronitrile (AIBN) and THF were purchased from Sigma-Aldrich (UK). HPLC-grade *n*-heptane and dichloromethane (DCM) were purchased from VWR (UK), while deuterated NMR solvents (CDCl<sub>3</sub> and CD<sub>2</sub>Cl<sub>2</sub>) were acquired from Sigma-Aldrich (UK) and Cambridge Isotope Laboratories (USA), respectively. Silica gel 60 (0.015-0.040 mm) for column chromatography was purchased from Merck Millipore (Germany). The DCM used for the macro-CTA synthesis was dried in-house using a Grubbs solvent purification system. The PETTC RAFT agent was synthesized according to a protocol reported elsewhere.<sup>66</sup> All other reagents were used as received.

### Synthesis of PDMS<sub>66</sub> macro-CTA

The macro-CTA was prepared via DCC/DMAP-catalysed esterification of the monocarbinol-terminated PDMS. PETTC (1.02 g; 3.0 mmol) was placed in a previously dried 250 ml round-bottomed flask and dissolved in DCM (100 ml). PDMS<sub>66</sub> (10.00 g; 2.0 mmol), DCC (1.20 g; 6.0 mmol) and DMAP (36.60 mg; 0.30 mmol) were then added and the resulting solution was purged with nitrogen for 15 minutes, sealed and heated for 20 h at reflux (~ 47 °C) with continuous stirring. After quenching the reaction by exposure to air, the solution was filtered, concentrated under vacuum with the aid of a rotary evaporator and passed through a silica gel column using DCM as eluent. The

resulting clear liquid was washed three times with a 2:1 methanol/DCM mixture and the organic layer was concentrated under vacuum to produce a clear yellow oil.

### **Synthesis of PDMS<sub>66</sub>-PBzMA<sub>x</sub> diblock copolymers via RAFT dispersion polymerization of PBzMA in *n*-heptane**

In a typical experiment, PDMS<sub>66</sub> macro-CTA (20.0 μmol; 0.10 g) and AIBN (0.70 mg, 4.0 μmol; added as a 0.70 mL of a 1.0 g dm<sup>-3</sup> initiator stock solution in *n*-heptane); macro-CTA/initiator molar ratio = 5.0), were weighed into a 10 ml vial. BzMA was added according to the desired DP, varying from 0.5 mmol (0.10 g) for DP = 25 up to 8 mmol (1.40 g) for DP = 400. An appropriate volume of *n*-heptane was then added, depending on the desired final solids content (10% to 30% w/v). After deoxygenation using nitrogen gas for 15 minutes at 0°C (using an ice bath) to avoid solvent evaporation, the vial was placed on a pre-heated oil bath at 70 °C and stirred for 20 h. Depending on the target DP of the PBzMA block and the desired solids content, the product was obtained as either a gel or a free-flowing dispersion.

### **Kinetics of PDMS<sub>66</sub>-PBzMA<sub>250</sub> synthesis via RAFT dispersion polymerization of BzMA in *n*-heptane**

To study the kinetics of the polymerization of BzMA at 25% solids, PDMS<sub>66</sub> macro-CTA (100 μmol; 0.50 g), AIBN (20 μmol; 3.3 mg; macro-CTA/initiator molar ratio = 5.0), BzMA (25 mmol; 4.40 g) and *n*-heptane (10.0 g) were added to a 20 ml round-bottom flask and deoxygenated with nitrogen gas for 30 min at 0°C (using an ice bath). The flask was placed in a pre-heated oil bath at 70°C to commence polymerization; at this point, the first aliquot was extracted via syringe. Multiple aliquots were taken over the first 8 h and finally after 23 h. These samples were characterized by <sup>1</sup>H NMR spectroscopy, THF GPC and DLS in order to assess the kinetics of polymerization and the evolution in copolymer molecular weight and particle size.

### **Characterization**

*Gel Permeation Chromatography (GPC)*. Molecular weight distributions were assessed using an Agilent PL-GPC 50 instrument equipped with two PLgel Mixed C 5 μm columns (300 x 7.5 mm). This instrument comprised a WellChrom Differential Refractometer K-2301 UV detector, a PD 2020 light scattering precision detector and a PL-BV400RT viscometer. The THF mobile phase was set at a flow rate of 1.0 ml min<sup>-1</sup> and comprised a solution of 2% v/v triethylamine and 0.05% w/v

butylhydroxytoluene. Ten poly(methyl methacrylate) calibration standards ranging from 1,280 to 330,000 g mol<sup>-1</sup> were used to construct the calibration plot.

*Proton Nuclear Magnetic Resonance (<sup>1</sup>H NMR) Spectroscopy.* Spectra were obtained using either a Bruker AV1 400 MHz 400 or a Bruker Avance DPX 400 MHz spectrometer. Sixty-four scans were averaged per spectrum and copolymer samples were dissolved in either CDCl<sub>3</sub> or CD<sub>2</sub>Cl<sub>2</sub>.

*Dynamic Light Scattering (DLS).* Hydrodynamic diameters were assessed using a Malvern Zetasizer Nano-ZS instrument at 25°C and a scattering angle of 173°. Copolymer dispersions were prepared at 0.1% in *n*-heptane. The mean diameters and polydispersities were calculated using Dispersion Technology Software version 6.20. This analysis assumes that all the colloidal aggregates have a spherical morphology.

*Transmission Electron Microscopy (TEM).* Images were obtained using a Philips CM 100 instrument at 100 kV equipped with a Gatan 1 k CCD camera. In-house surface-coated copper/palladium grids were used to support the samples (11 µl of 0.1% dispersion in *n*-heptane). The grids were allowed to dry for 10 min before staining them with ruthenium(IV) oxide vapor for 7 min at 20 °C. The protocol for the synthesis of the staining agent is described elsewhere.<sup>67</sup>

*UV Absorption Spectroscopy.* The mean degree of functionalization of the PDMS macro-CTA were assessed using a PerkinElmer Lambda 25 instrument to record spectra from 190 nm to 500 nm. A calibration plot was constructed from eight PETTC solutions of known concentration in dichloromethane with concentrations ranging from 1.0 x 10<sup>-4</sup> mol dm<sup>-3</sup> to 6 x 10<sup>-6</sup> mol dm<sup>-3</sup>. From this linear plot, an extinction coefficient of 10,720 ± 120 mol<sup>-1</sup> dm<sup>3</sup> cm<sup>-1</sup> was obtained which could be used to calculate the PDMS-PETTC end-group functionality. In order to determine the calibration error, three independent sets of standard solutions were measured. The mean degree of esterification of the PDMS macro-CTA was determined from an average of four spectroscopic measurements.

*Small-Angle X-ray Scattering (SAXS).* SAXS patterns were collected at a synchrotron source (ESRF, station BM26, Grenoble, France), using monochromatic X-ray radiation (wavelength, λ = 0.1 nm) and a 2D Pilatus 1M CCD detector. Data collection corresponded to a *q* range from 0.023 to 1.3 nm<sup>-1</sup>, where the scattering vector is given by  $q = 4\pi\sin\theta/\lambda$  and θ corresponds to one-half of the scattering angle. Copolymer dispersions prepared at either 1.0, 3.0 or 5.0% w/w in *n*-heptane were injected into a thin-walled flow-through quartz capillary cell. Scattering data were reduced by Nika SAS

macros for Igor Pro (integration, normalization, and background subtraction) and were further analyzed using Irena SAS macros for Igor Pro.<sup>68</sup> Glassy carbon was used for the absolute intensity calibration.<sup>69</sup>

## Results and Discussion

An important advantage of using commercially available polymers as precursors for the preparation of RAFT macro-CTAs is that the same mean degree of polymerization can be consistently obtained, which is not necessarily the case for the various (meth)acrylic macro-CTAs previously utilized for dispersion polymerization formulations.<sup>47,48,50,54,55,70-76</sup> For example, we recently reported the reaction of monoamine-functionalized PEG<sub>113</sub> with an activated ester-based RAFT agent to form a monofunctional PEG<sub>113</sub> macro-CTA.<sup>77</sup> This amidation route was chosen because the alternative esterification reaction is rather less efficient when conducted in aqueous solution. Moreover, the amide bond is much less susceptible to hydrolysis under physiological conditions, which is desirable for potential biomedical applications.<sup>78</sup>

In contrast, the PISA formulation described herein involves a non-polar solvent (*n*-heptane), hence an ester bond should provide sufficient chemical stability. It is known that DMAP catalysis of the DCC-activated esterification of carboxylic acids is highly efficient when conducted in non-aqueous media, provided that the reagents are rigorously purified in order to remove protic impurities such as water. Addition of DMAP also suppresses the formation of side-products commonly found in the uncatalyzed reaction.<sup>78,79</sup> In the case of the monocarbinol-terminated PDMS utilized herein, the long-chain nature of the nucleophile can be problematic, since the reactivity of the terminal hydroxy end-group can be reduced. Thus esterification was conducted in DCM under reflux, which yielded a PDMS<sub>66</sub> macro-CTA that was analyzed by <sup>1</sup>H NMR and UV absorption spectroscopy. It was possible to assign the PDMS<sub>66</sub> macro-CTA spectrum by comparison to that of PETTC and the PDMS<sub>66</sub>-OH precursor (see Figure 1). The mean degree of end-group functionalization was determined by comparing the integrated backbone dimethyl protons at 0.1 ppm (labelled *m*, *n* and *o* in Figure 1b) with three sets of protons associated with the PETTC end-group. The latter signals consisted of the five aromatic protons at 7.5 ppm, (labeled *a*, *b* and *c* in Figure 1a), the two benzyl protons at 3.0 ppm (labeled *e*), and the methylene protons (labeled *g* and *h*). Thus a mean degree of esterification of 94 ± 1 % was calculated. This relatively high degree of end-group functionalization was confirmed by UV absorption spectroscopy. Briefly, an absorbance vs. concentration plot was constructed using various known solutions of PETTC in DCM. In this case, the PETTC closely resembles the RAFT end-group that is conjugated to the PDMS chain, which is a prerequisite for reliable end-group analysis

using this technique.<sup>80</sup> From the calibration plot, a mean extinction coefficient,  $\epsilon$ , of  $10,717 \pm 119 \text{ mol}^{-1} \text{ dm}^3 \text{ cm}^{-1}$  was calculated for the absorption maximum at 300 nm (see Supporting Information, Figure S1). Using this  $\epsilon$  value in conjunction with the absorbance  $A$  recorded for various PDMS<sub>66</sub> macro-CTA solutions of known concentration  $c$  enabled a degree of end-group functionalization of  $92 \pm 2 \%$  to be calculated using the Beer-Lambert equation  $A = \epsilon \cdot c \cdot l$  (where  $l$  is the path length of the UV cell). Within experimental error, this value is consistent with that determined by <sup>1</sup>H NMR spectroscopy. Such end-group fidelity is likely to be comparable to that achieved for (meth)acrylic macro-CTAs prepared by RAFT solution polymerization for other PISA syntheses.<sup>46</sup> Moreover, the use of a commercial PDMS precursor should ensure consistent batch-to-batch reproducibility for the molecular weight of the macro-CTA, which is highly desirable for the construction of phase diagrams (see below).

This PDMS<sub>66</sub> macro-CTA was subsequently used for the RAFT dispersion polymerization of BzMA in *n*-heptane at 70 °C. A kinetic study performed for a target diblock composition of PDMS<sub>66</sub>-PBzMA<sub>250</sub> at 25% solids (macro-CTA/initiator molar ratio = 5.0) indicated an initial induction period of around 30 min (commonly observed for RAFT syntheses)<sup>81</sup>, followed by the relatively slow polymerization of BzMA. According to the semi-logarithmic plot shown in Figure 2a, a six-fold increase in the rate of polymerization is observed at around 30 % conversion, which corresponds to a mean PBzMA DP of 75. According to previous RAFT dispersion polymerization studies, this most likely indicates the onset of micellar nucleation.<sup>46,72,82</sup> The semi-logarithmic plot in the latter regime remained linear up to approximately 90 % conversion, with a reduction in the rate of polymerization being observed thereafter.

Aliquots extracted during the kinetic study were also analyzed by THF GPC, which confirmed the linear evolution of  $M_n$  with monomer conversion (Figure 2b). Moreover, each GPC curve proved to be unimodal and a relatively high blocking efficiency for the PDMS<sub>66</sub> macro-CTA was observed.  $M_w/M_n$  values were around 1.25 at low conversions and fell to 1.18 as the BzMA polymerization progressed. Such a reduction is expected for a living polymerization with little or no termination.<sup>83</sup> This excellent living character contrasts markedly with observations made by Fielding et al. for the RAFT polymerization of BzMA in *n*-heptane using a poly(lauryl methacrylate) macro-CTA.<sup>46</sup> Molecular weight distributions broadened significantly at higher monomer conversions in this earlier study, indicating progressive loss of control.

DLS studies on the kinetic samples (Figure 3) indicated the presence of spheres with intensity-diameters of 28-31 nm and relatively low polydispersities at 18-28 % BzMA conversion. However, a

significant increase up to 140 nm diameter (with an associated increase in polydispersity from 0.09 to 0.21) was observed from 39 % to 51 % conversion, suggesting a change in the copolymer morphology. According to TEM studies (see Figure 3) a mixed phase of worms and spheres is formed within this range of conversions. Higher conversions led to a slightly lower sphere-equivalent diameter of 130 nm, with a concomitant significant reduction in polydispersity to 0.08. TEM studies of samples extracted during the latter stages of the BzMA polymerization indicate that this final copolymer morphology corresponds to vesicles (see Figure 3 and Figure S3). Similar observations regarding the *in situ* evolution of copolymer morphology during PISA formulations were reported by Blanz et al.<sup>82</sup>

The effect of varying both the target PBzMA DP and the solids concentration on the morphology of the resulting PDMS<sub>66</sub>-PBzMA<sub>x</sub> nano-objects was investigated by targeting a series of diblock copolymers, which were characterized by <sup>1</sup>H NMR spectroscopy, DLS, TEM, THF GPC and, in selected cases, SAXS. According to <sup>1</sup>H NMR studies performed on the diluted reaction solutions, the final BzMA conversions ranged from 90% to 100%. *Post mortem* THF GPC studies (see Figure 4) confirmed systematic increases in  $M_n$  when targeting higher DPs and consistently low final polydispersities ( $M_w/M_n = 1.14 - 1.34$ ). Similar GPC data have been reported for various other PISA formulations.<sup>54,70,71,82</sup>

According to DLS and TEM studies, only spherical nanoparticles were obtained when the polymerization was conducted at either 10 or 15% solids, regardless of the targeted diblock composition. SAXS was also used to characterize these spherical nanoparticles, with the scattering patterns featuring the expected zero gradient at low  $q$  (Guinier regime, see Figure 5a).<sup>46,54,76,84</sup> The minima observed at higher  $q$  contain particle size information. As the target DP of the core-forming PBzMA block is systematically increased from 24 to 285, the first minimum gradually shifts to lower  $q$ , indicating a progressive increase in sphere dimensions. Fitting these data to a well-known spherical micelle model,<sup>85,86</sup> the volume-average diameter,  $D_v$ , can be determined. The calculated  $D_v$  values increased monotonically from 16 nm to 45 nm (see Figure 5b) and SAXS analysis indicated relatively narrow size distributions in each case ( $\pm 10\%$ ). On the other hand, DLS reports an intensity-average particle diameter, which also increases monotonically with target PBzMA DP (see Figure 5b). This is consistent with previous PISA syntheses involving the RAFT dispersion polymerization of BzMA in either polar or non-polar media, where the mean spherical particle diameter was strongly correlated with the DP of the core-forming block. It is perhaps worth emphasizing here that SAXS always undersizes relative to DLS, simply because these techniques report differing moments of the particle size distribution.

A further series of PDMS<sub>66</sub>-PBzMA<sub>x</sub> diblock copolymer nano-objects were synthesized via RAFT dispersion polymerization in which the solids content and target x values were varied in order to construct a detailed phase diagram. Here the final copolymer morphology was assigned on the basis of *post mortem* TEM studies (see Figure 6). Conducting the BzMA polymerization at higher solids ( $\geq 20\%$ ) yielded spheres for  $x = 25$ , whereas higher order morphologies were observed when targeting  $x \geq 50$ . When  $x = 50 - 90$ , the resulting viscous liquids consisted of mixed phases of spheres and worms. A pure vesicle phase was obtained when targeting  $x = 150 - 300$  at 20 % w/v solids – such dispersions are typically free-flowing and relatively turbid. However, it was necessary to increase the solids content to 25 % w/v for  $x = 80$  in order to obtain a pure worm phase, which formed a free-standing gel. When targeting  $x = 50 - 70$ , either free-standing gels or viscous liquids comprising mixed phases of spheres and worms were obtained, whereas mixed phases of spheres and vesicles were observed where  $x = 90 - 110$ . The minimum value of x required for a pure vesicle phase was lowered to 120 at 25 % w/v solids and was further reduced to 100 at 30 % w/v solids. This is a common observation for such RAFT-mediated PISA formulations; higher concentrations significantly increase the probability of fusion events between the growing monomer-swollen particles, which are essential for the *in situ* evolution in nano-object morphology.<sup>73</sup> In contrast, if inter-particle collisions remain elastic, or are simply too infrequent on the time scale of the polymerization, this results in the formation of kinetically-trapped spheres.<sup>76</sup> In the present study, such kinetically-trapped spheres are readily identified when targeting higher PBzMA DPs on the left-hand side of the phase diagram shown in Figure 6, since targeting precisely the same diblock composition at higher solids leads to the thermodynamically-favored copolymer morphology (e.g. vesicles). One particularly striking feature of this phase diagram is the remarkably narrow worm phase region. Similar observations have been recently made for other PISA formulations based on RAFT dispersion polymerization.<sup>87</sup> It is well-known that the precise position of the boundaries in such PISA phase diagrams can be quite sensitive to the nature of the solvent.<sup>88</sup> Thus the phase diagram shown in Figure 5 is likely to be subtly different on switching from *n*-heptane to other *n*-alkanes.

SAXS studies were also conducted on PDMS<sub>66</sub>-PBzMA<sub>80</sub> worms and PDMS<sub>66</sub>-PBzMA<sub>400</sub> vesicles (see Figure 7). The scattering curve obtained for the worms exhibits a gradient of approximately -1 in the Guinier regime, which is characteristic for such highly anisotropic particles.<sup>84</sup> In principle, fitting this SAXS pattern to a worm-like micelle model previously validated for PLMA-PBzMA worms in *n*-alkanes<sup>59</sup> enables both the mean worm cross-section and average worm contour length to be extracted. A value of 26 nm was calculated for the former parameter, with a reasonably good data fit being achieved. As a comparison, mean diameters of 21 nm and 27 nm were determined for PDMS<sub>66</sub>-PBzMA<sub>50</sub> and PDMS<sub>66</sub>-PBzMA<sub>100</sub> spheres, respectively. Thus a worm cross-section of 26 nm

for PDMS<sub>66</sub>-PBzMA<sub>80</sub> worms seems to be physically reasonable and is comparable to the worms observed in the TEM image in Figure 6a. Unfortunately, only a *lower limit* value of around 1000 nm could be determined for the mean worm contour length from the same data fit. Despite the relatively long camera length available at the synchrotron X-ray facility, the accessible  $q$  range was not sufficiently low to provide more accurate information.

The scattering curve obtained for the PDMS<sub>66</sub>-PBzMA<sub>400</sub> vesicles also proved to be information-rich. This pattern was fitted using a typical core-shell model with an additional parameter to account for the polydispersity of the membrane.<sup>89</sup> The low  $q$  feature corresponds to the overall vesicle dimensions. A volume-average vesicle diameter of 315 nm was calculated from the data fit, which is in reasonable agreement with the intensity-average diameter of 371 nm indicated by DLS. Again, some discrepancy between these two values is to be expected given the differing moments reported by SAXS and DLS. The high  $q$  feature corresponds to the mean membrane thickness, for which a value of 36 nm is calculated from the data fit. This is comparable to that estimated from the TEM images shown in Figure 6a.

Finally, the 30 % w/v PDMS<sub>66</sub>-PBzMA<sub>80</sub> worm gel was further characterized without further dilution by rheology measurements performed at 25 °C. A plateau in the strain sweep confirmed the viscoelastic nature of this gel. Increasing the applied strain beyond 10 % reduces  $G'$  below  $G''$ , which denotes the Bingham yield stress. At this point, it is likely that the multiple inter-worm contacts within the gel are disrupted, thus causing degelation. An experiment was also conducted in order to assess the effect of applied frequency on the dynamic gel viscosity. The gel viscosity is reduced at higher frequency, indicating shear-thinning behavior. Similar observations have also been reported for aqueous diblock copolymer worm gels prepared using PISA formulations.<sup>90</sup> Unfortunately, the relatively low boiling point of *n*-heptane (98 °C) precludes variable temperature studies over a sufficiently wide range (up to 150 °C)<sup>50</sup> to investigate whether the present PDMS<sub>66</sub>-PBzMA<sub>80</sub> worm gel exhibit thermo-responsive behavior, e.g. degelation via a worm-to-sphere transition, as recently reported for a PLMA-PBzMA diblock copolymer PISA formulation.<sup>59</sup> Such experiments would most likely require identification of a pure worm phase in a much less volatile solvent such as *n*-dodecane.

## Conclusions

A well-defined PDMS<sub>66</sub> macro-CTA with a high degree of functionality was synthesized via esterification of a monocarbinol-terminated PDMS using PETTC. This near-monodisperse macro-CTA was used to prepare a series of PDMS<sub>66</sub>-PBzMA<sub>x</sub> diblock copolymers via RAFT dispersion

polymerization of BzMA in *n*-heptane. The kinetics of the polymerization were similar to that previously reported for such PISA formulations, while the linear evolution of  $M_n$  with conversion and relatively low final polydispersities confirmed its living character. TEM and DLS analyses indicated a gradual evolution in copolymer morphology from spheres to a mixed sphere/worm phase to vesicles with increasing conversion. Systematic variation of both the diblock composition and the solids content enabled the identification of pure phases comprising spheres, worms or vesicles. Spheres were obtained at or below 20 % w/v solids, with mean hydrodynamic diameters ranging from 25 to 55 nm as the target PBzMA DP was increased (as judged by DLS and TEM studies). Vesicles could be prepared by targeting PBzMA DPs greater than 175 when working at 20 % w/v solids or above. A pure worm phase was identified for just two formulations: a PDMS<sub>66</sub>-PBzMA<sub>80</sub> diblock copolymer prepared at either 25 % or 30 % w/v solids. Both dispersions formed fairly transparent free-standing gels. It is perhaps noteworthy that other diblock copolymer compositions targeted at the same solids also formed free-standing gels, but TEM studies indicated that these formulations were composed of mixed phases, rather than a pure worm phase.

Selected PDMS<sub>66</sub>-PBzMA<sub>x</sub> dispersions were also analyzed by SAXS. The mean diameter of the series of PDMS<sub>66</sub>-PBzMA<sub>x</sub> spheres prepared at 10 % w/v solids increased systematically with PBzMA DP, with a similar correlation being indicated by DLS studies. SAXS studies of PDMS<sub>66</sub>-PBzMA<sub>80</sub> worms revealed a mean worm cross-section of 26 nm and a mean worm contour length of at least 1000 nm. PDMS<sub>66</sub>-PBzMA<sub>400</sub> vesicles prepared at 25 % w/v solids were also characterized by SAXS. In this case the volume-average vesicle diameter of 315 nm calculated from the data fit was comparable to the intensity-average diameter of 370 nm indicated by DLS studies. A mean vesicle membrane thickness of 36 nm was also determined, which is comparable to that indicated by TEM studies.

Ambient temperature rheology studies performed on the PDMS<sub>66</sub>-PBzMA<sub>80</sub> worm gel prepared at 30 % w/v solids indicated viscoelastic behavior up to an applied strain of 1 %. This gel also exhibited shear-thinning behavior, which has been observed for other diblock copolymer worm gels.

**Acknowledgments.** CONACYT is acknowledged for funding an MSc studentship for APL. EPSRC is thanked for post-doctoral support of NJW (Platform grant EP/J007846/1). SPA acknowledges a five-year ERC Advanced Investigator grant (PISA 320372).

## List of Schemes

**Scheme 1.** Synthesis of PDMS<sub>66</sub> macro-CTA via DDC/DMAP-catalyzed esterification of monocarbinol-terminated PDMS using a carboxylic acid-functionalized RAFT agent (PETTC) followed by synthesis of PDMS<sub>66</sub>-PBzMA<sub>x</sub> via RAFT dispersion polymerization of benzyl methacrylate (BzMA) in *n*-heptane using AIBN initiator at 70°C.

## List of Figures

**Figure 1.** <sup>1</sup>H NMR spectra recorded in CD<sub>2</sub>Cl<sub>2</sub> for (a) PETTC chain transfer agent precursor, (b) monocarbinol PDMS<sub>66</sub> precursor, (c) PDMS<sub>66</sub> macro-CTA and (d) PDMS<sub>66</sub>-PBzMA<sub>100</sub> diblock copolymer.

**Figure 2.** (a) Kinetic data obtained for a RAFT dispersion polymerization of BzMA using AIBIN initiator at 70 °C in *n*-heptane at 25% w/v solids when targeting PDMS<sub>66</sub>-PBzMA<sub>250</sub> composition and using a PDMS<sub>66</sub> macro-CTA/AIBN molar ratio of 5.0. The onset of micellar nucleation corresponds to the point at which the polymerization rate shows a distinctive change in slope at around 3.5 h. The linear form of this semi-logarithmic plot indicates first-order kinetics with respect to BzMA monomer from 3.5 h to 6 h, which corresponds to 40% - 90% conversion. (b) Evolution of M<sub>n</sub> (blue data) and M<sub>w</sub>/M<sub>n</sub> (red data) with conversion as judged by THF GPC.

**Figure 3.** Selected TEM images, particle diameter and associated polydispersity data obtained via dynamic light scattering measurements carried out on samples extracted from a kinetic study of the polymerization of BzMA using the PDMS<sub>66</sub> macro-CTA at 25 % w/v solids.

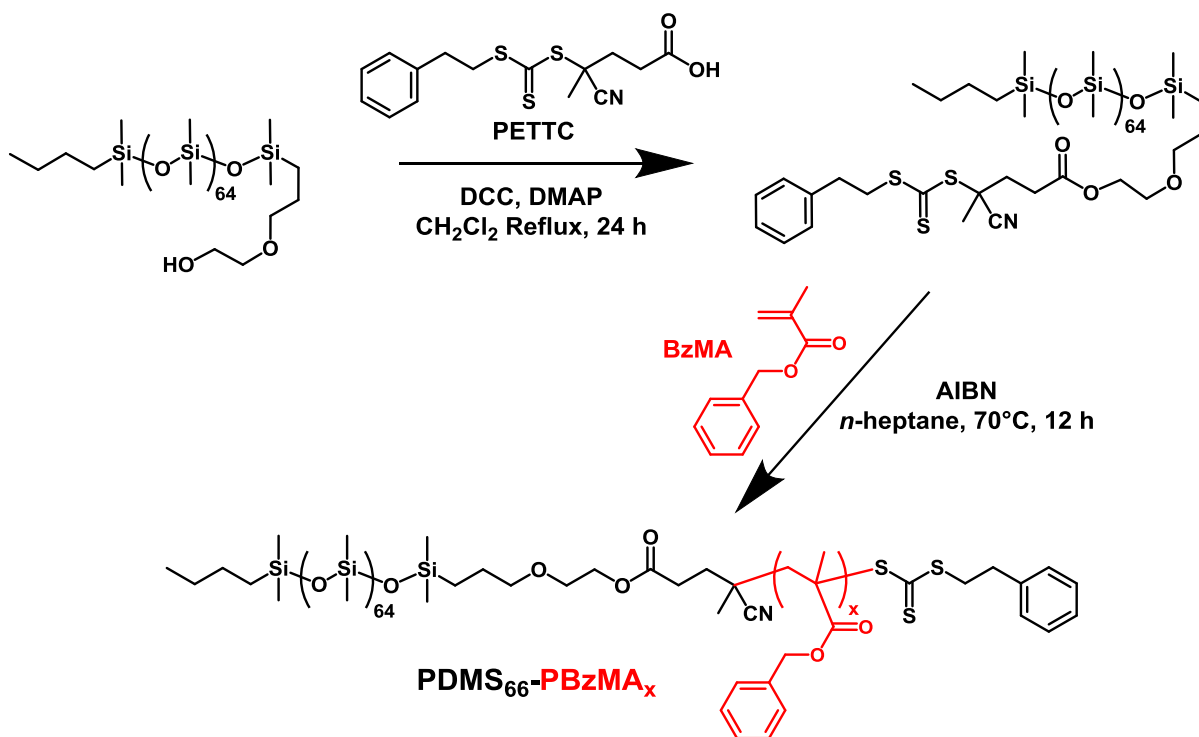
**Figure 4.** (a) Normalized GPC curves for a series of PDMS<sub>66</sub>-PBzMA<sub>x</sub> diblock copolymers prepared at 15% w/v solids as judged by THF GPC. Each block copolymer was synthesized by chain extension of a PDMS<sub>66</sub> macro-CTA (see dashed black line) via RAFT dispersion polymerization of BzMA conducted in *n*-heptane at 70 °C, with high conversions (> 95 %) being achieved in each case.

**Figure 5.** (a) SAXS patterns obtained for a series of PDMS<sub>66</sub>-PBzMA<sub>x</sub> diblock copolymer spheres (where x = 24, 49, 98, 144, 188, 243 or 282) prepared via RAFT dispersion polymerization of BzMA in *n*-heptane at 10% w/v solids. (b) Relationship between particle size (volume-average diameter, D<sub>v</sub>, determined by SAXS or Intensity-average diameter, D<sub>i</sub>, determined by DLS) and target degree of polymerization of the core-forming PBzMA block for a series of PDMS<sub>66</sub>-PBzMA<sub>x</sub> diblock copolymer spheres prepared via RAFT dispersion polymerization of BzMA in *n*-heptane at 10% w/v solids.

**Figure 6.** (a) Representative TEM images for PDMS<sub>66</sub>-PBzMA<sub>x</sub> diblock copolymers at 25% w/v solids. Spherical aggregates are formed when relatively low PBzMA DPs are targeted, whereas worms and vesicle morphologies are observed at higher PBzMA DP values. (b) Phase diagram constructed for PDMS<sub>66</sub>-PBzMA<sub>x</sub> diblock copolymers prepared via RAFT dispersion polymerization of BzMA in *n*-heptane at 70 °C using AIBN initiator. Diblock copolymer morphologies were assigned by TEM analysis and mean PBzMA DP values were calculated from the diblock composition determined by <sup>1</sup>H NMR spectroscopy in CD<sub>2</sub>Cl<sub>2</sub>.

**Figure 7.** SAXS curves (black data; recorded at 1.0 % w/v solids) recorded for PDMS<sub>66</sub>-PBzMA<sub>80</sub> worms and PDMS<sub>66</sub>-PBzMA<sub>300</sub> vesicles originally synthesized at 25 % w/v solids in *n*-heptane via RAFT dispersion polymerization of BzMA at 70 °C. Fits to these curves are shown as red lines when using an appropriate worm<sup>50</sup> or vesicle<sup>76</sup> model, respectively. Inset cartoons depict the respective nano-object dimensions as extracted from the relevant model.

**Figure 8.** (a) Dependence of the applied strain on the storage ( $G'$ ) and loss ( $G''$ ) moduli and (b) frequency dependence of the complex viscosity ( $\eta^*$ ) for a 30 % w/v dispersion of PDMS<sub>66</sub>-PBzMA<sub>80</sub> worms in *n*-heptane at 25°C.



**Scheme 1.** Synthesis of PDMS<sub>66</sub> macro-CTA via DCC/DMAP-catalyzed esterification of monocarbinol-terminated PDMS using a carboxylic acid-functionalized RAFT agent (PETTC) followed by synthesis of PDMS<sub>66</sub>-PBzMA<sub>x</sub> via RAFT dispersion polymerization of benzyl methacrylate (BzMA) in *n*-heptane using AIBN initiator at 70°C.

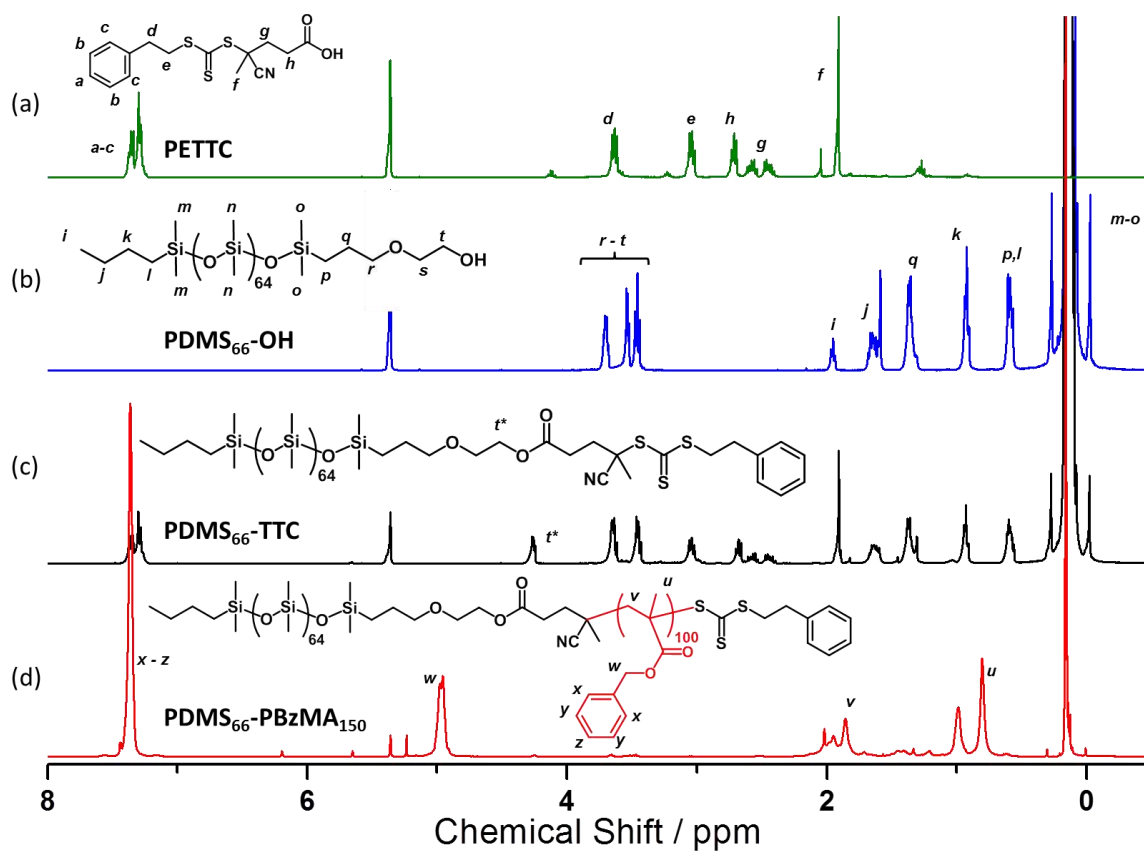


**Figure 1.**  $^1\text{H}$  NMR spectra recorded in  $\text{CD}_2\text{Cl}_2$  for (a) PETTC chain transfer agent precursor, (b) mono-carbinol PDMS<sub>66</sub> precursor, (c) PDMS<sub>66</sub> macro-CTA and (d) PDMS<sub>66</sub>-PBzMA<sub>150</sub> diblock copolymer.

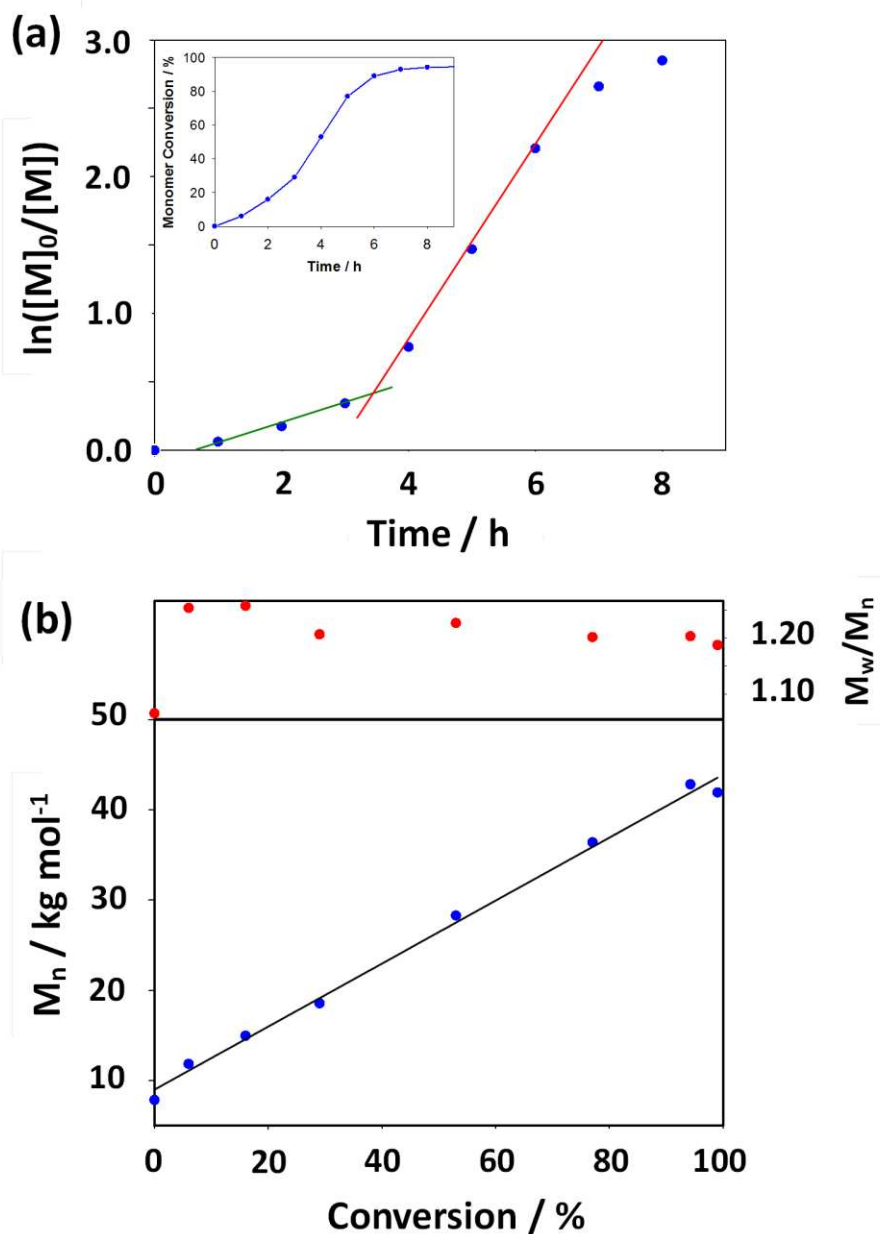


**Figure 2.** (a) Kinetic data obtained for a RAFT dispersion polymerization of BzMA using AIBIN initiator at 70 °C in *n*-heptane at 25% w/v solids when targeting PDMS<sub>66</sub>-PBzMA<sub>250</sub> composition and using a PDMS<sub>66</sub> macro-CTA/AIBN molar ratio of 5.0. The onset of micellar nucleation corresponds to the point at which the polymerization rate shows a distinctive change in slope at around 3.5 h. The linear form of this semi-logarithmic plot indicates first-order kinetics with respect to BzMA monomer from 3.5 h to 6 h, which corresponds to 40% - 90% conversion. (b) Evolution of  $M_n$  (blue data) and  $M_w/M_n$  (red data) with conversion as judged by THF GPC.

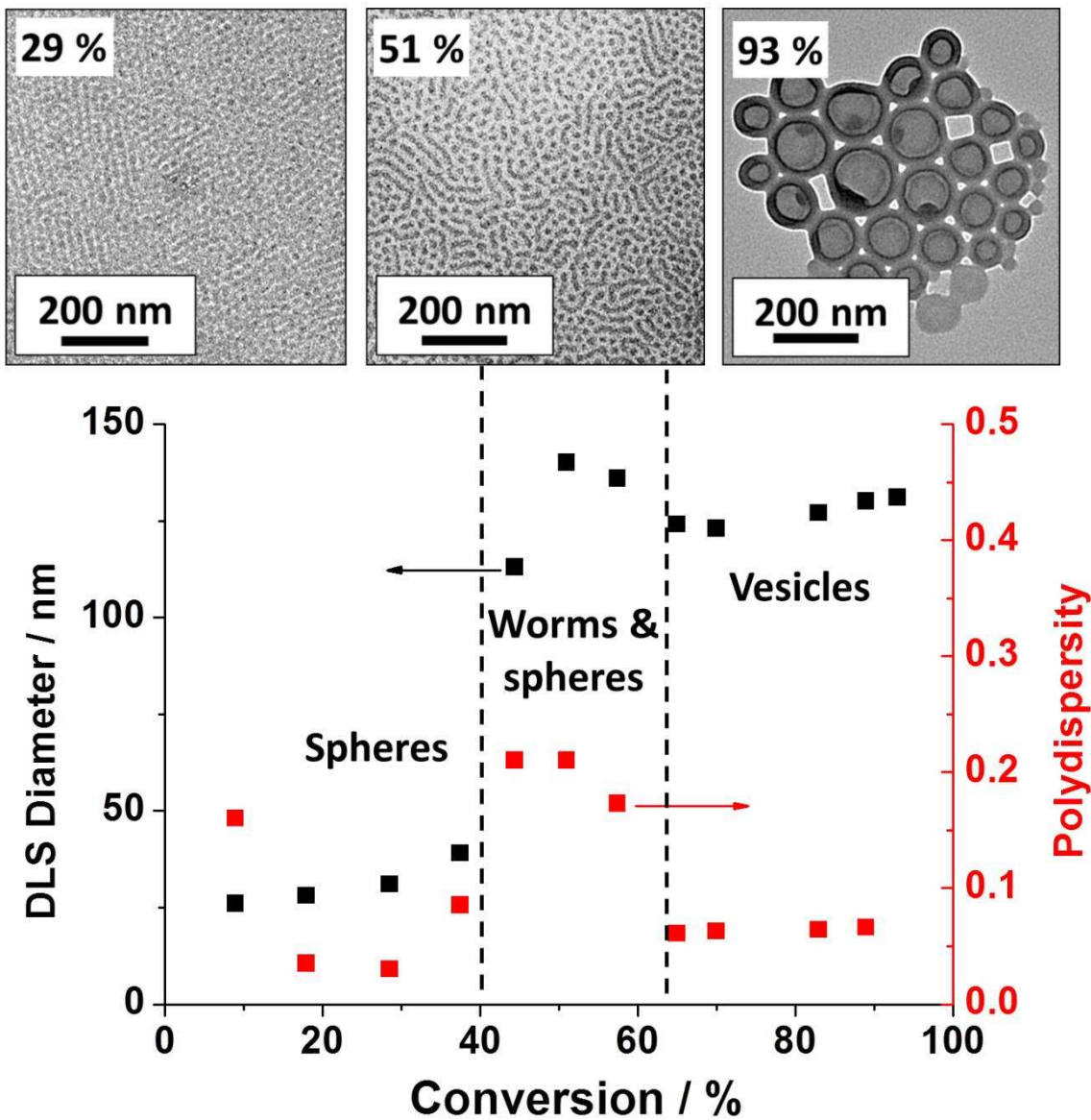


**Figure 3.** Selected TEM images, particle diameter and associated polydispersity data obtained via dynamic light scattering measurements carried out on samples extracted from a kinetic study of the polymerization of BzMA using the PDMS<sub>66</sub> macro-CTA at 25 % w/v solids.

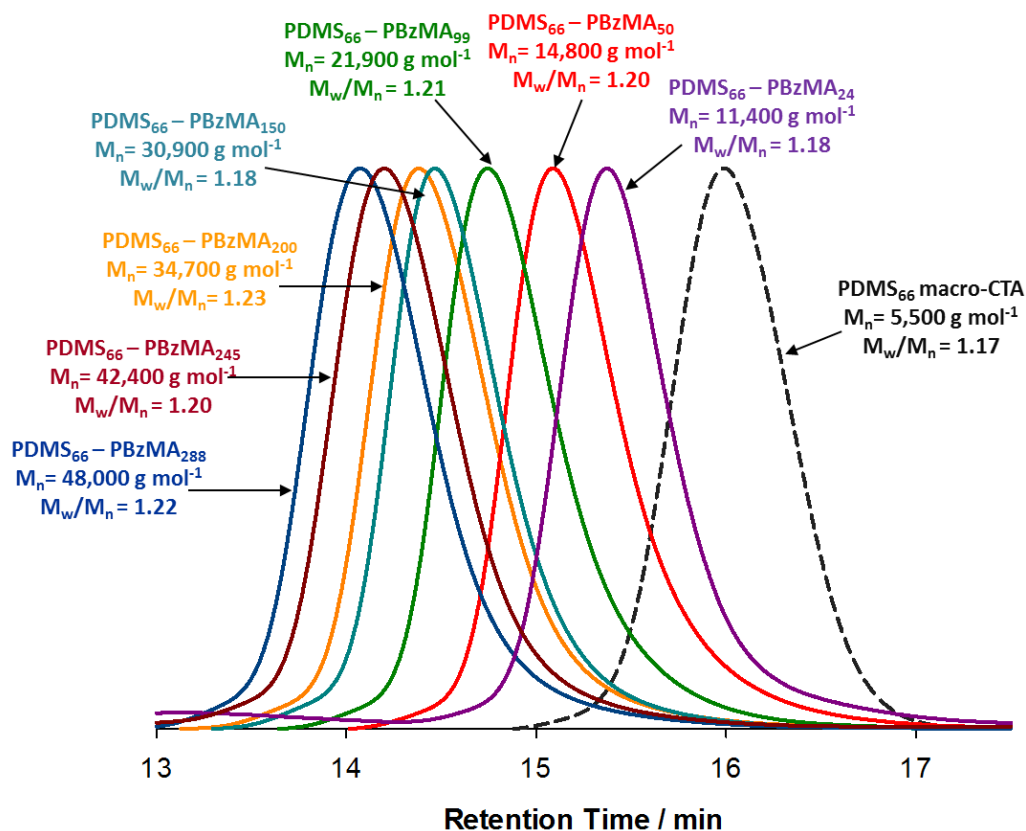


**Figure 4.** Normalized GPC curves for a series of PDMS<sub>66</sub>-PBzMA<sub>x</sub> diblock copolymers prepared at 15% w/v solids as judged by THF GPC using RI detection. Each block copolymer was synthesized by chain extension of a PDMS<sub>66</sub> macro-CTA (see dashed black line) via RAFT dispersion polymerization of BzMA conducted in *n*-heptane at 70 °C, with high conversions (> 95 %) being achieved in each case.

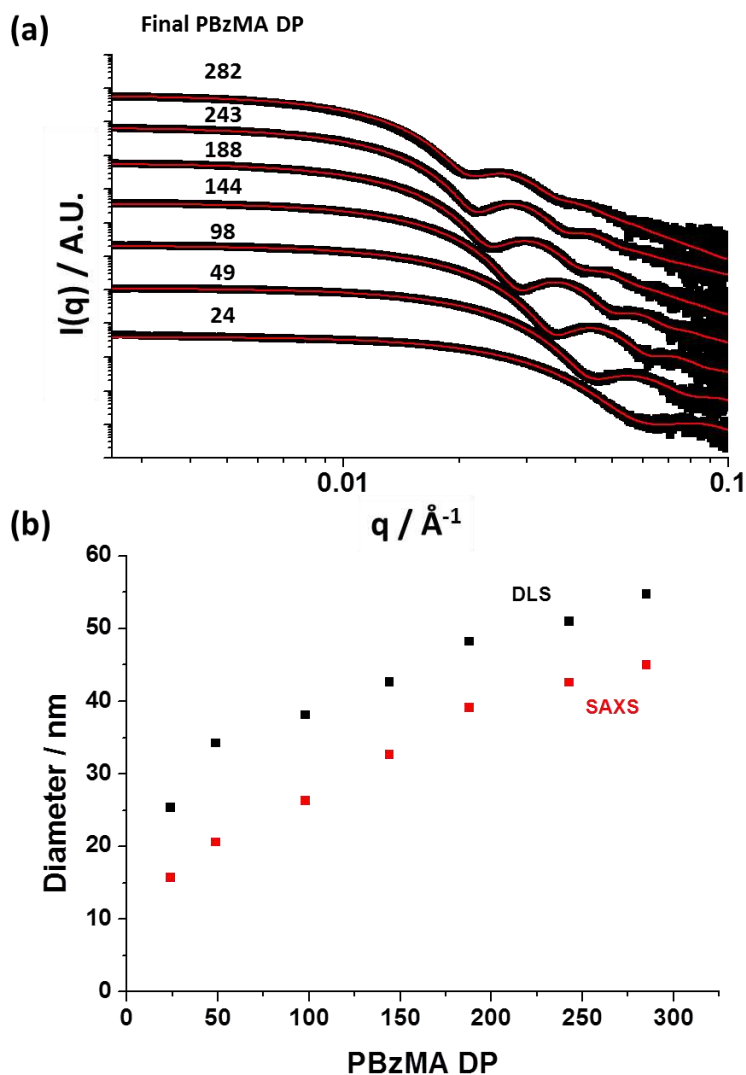


**Figure 5.** (a) SAXS patterns obtained for a series of PDMS<sub>66</sub>-PBzMA<sub>x</sub> diblock copolymer spheres (where  $x = 24, 49, 98, 144, 188, 243$  or  $282$ ) prepared via RAFT dispersion polymerization of BzMA in *n*-heptane at 10% w/v solids. (b) Relationship between particle size (volume-average diameter,  $D_v$ , determined by SAXS or Intensity-average diameter,  $D_i$ , determined by DLS) and target degree of polymerization of the core-forming PBzMA block for a series of PDMS<sub>66</sub>-PBzMA<sub>x</sub> diblock copolymer spheres prepared via RAFT dispersion polymerization of BzMA in *n*-heptane at 10% w/v solids.

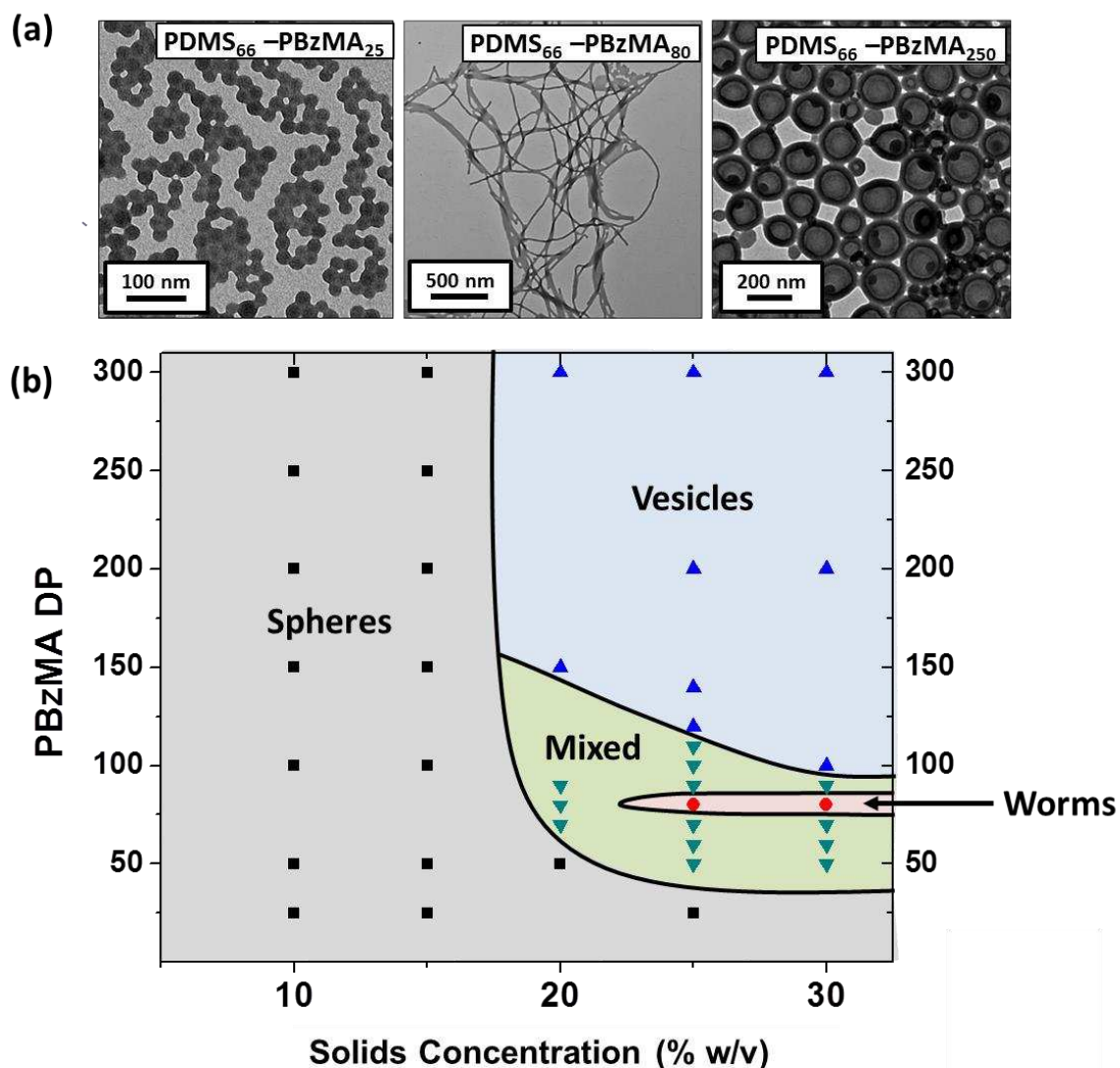


**Figure 6.** (a) Representative TEM images for PDMS<sub>66</sub>-PBzMA<sub>x</sub> diblock copolymers at 25% w/v solids. Spherical aggregates are formed when relatively low PBzMA DPs are targeted, whereas worms and vesicle morphologies are observed at higher PBzMA DP values. (b) Phase diagram constructed for PDMS<sub>66</sub>-PBzMA<sub>x</sub> diblock copolymers prepared via RAFT dispersion polymerization of BzMA in *n*-heptane at 70 °C using AIBN initiator. Diblock copolymer morphologies were assigned by TEM analysis and mean PBzMA DP values were calculated from the diblock composition determined by <sup>1</sup>H NMR spectroscopy in CD<sub>2</sub>Cl<sub>2</sub>.

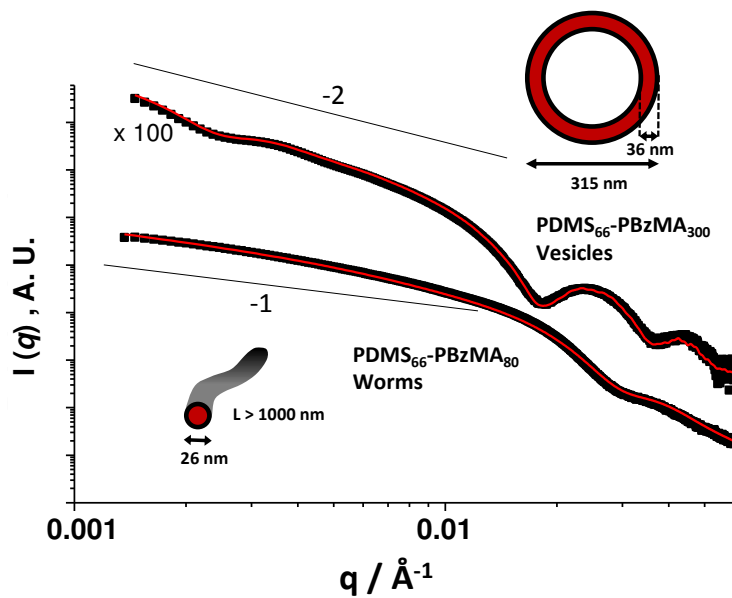


**Figure 7.** SAXS curves (black data; recorded at 1.0 % w/v solids) recorded for PDMS<sub>66</sub>-PBzMA<sub>80</sub> worms and PDMS<sub>66</sub>-PBzMA<sub>300</sub> vesicles originally synthesized at 25 % w/v solids in *n*-heptane via RAFT dispersion polymerization of BzMA at 70 °C. Fits to these curves are shown as red lines when using an appropriate worm<sup>50</sup> or vesicle<sup>76</sup> model, respectively. Inset cartoons depict the respective nano-object dimensions as extracted from the relevant model.

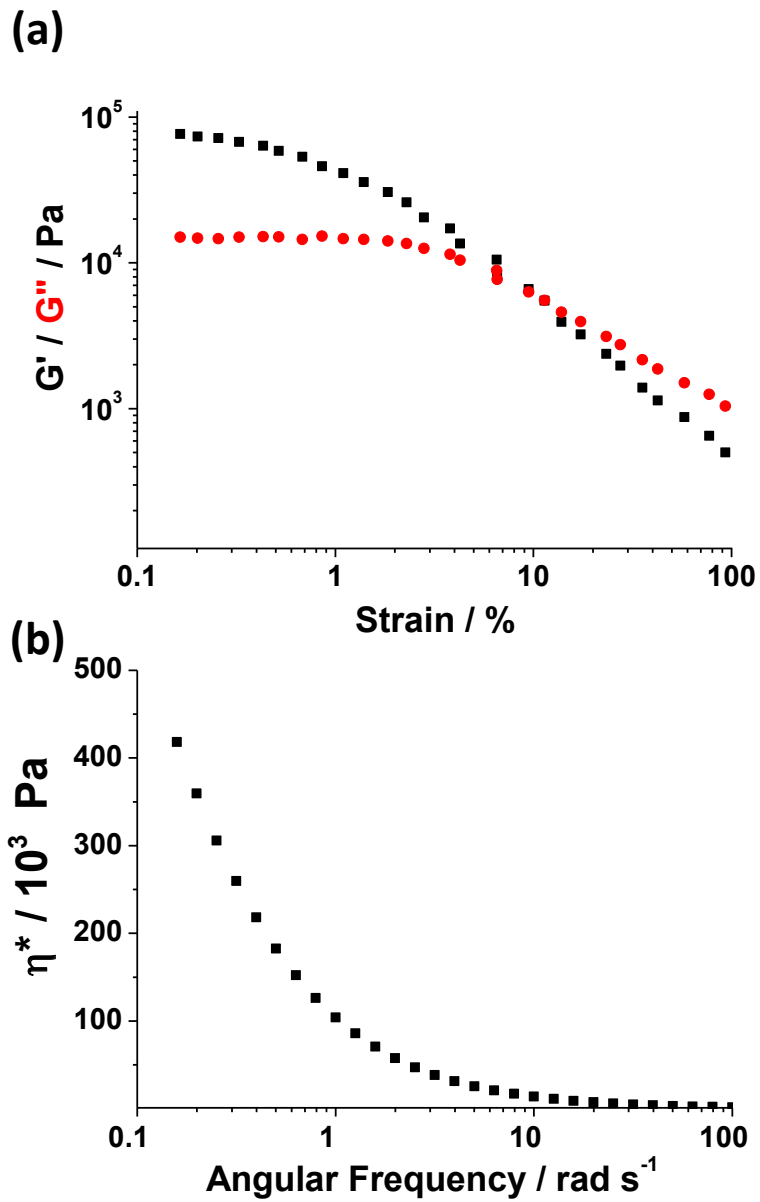


**Figure 8.** (a) Dependence of the applied strain on the storage ( $G'$ ) and loss ( $G''$ ) moduli and (b) frequency dependence of the complex viscosity ( $\eta^*$ ) for a 30 % w/v dispersion of PDMS<sub>66</sub>-PBzMA<sub>80</sub> worms in *n*-heptane at 25°C.

## References

- (1) Owen, M. J. *Siloxane Surface-Activity*; American Chemical Society: Washington, 1990; Vol. 224.
- (2) Yilgör, E.; Yilgör, I. *Progress in Polymer Science* **2014**, *39*, 1165.
- (3) Cooper, E. C.; Welch, R. J.; The Procter & Gamble Company 1998.
- (3) Cooper, E. C.; Welch, R. J. Hair cosmetic compositions, The Procter & Gamble Company, US patent no. 5811109, 1998.
- (4) Davy, P. F.; Drolet, M. L. Terminal aminofunctional polysiloxane hair conditioning compositions and their use in hair colouring compositions, The Procter & Gamble Company, Eur. patent no. EP 1392227, 1978.
- (5) Favreau, V. Cosmetic composition useful for treating keratin fibers comprises at least one copolymer based on silicone resin and on silicone fluid, at least one silicone surfactant, and a non-volatile linear polydimethylsiloxane, L'Oréal, WO2011117403-A2, 2012.
- (6) Breitenbach J.; Lefebvre D. R.; Lipari J. M. Nanosuspension formulation used in pharmaceutical, cosmetics and food industry, comprises particles of at least one functional ingredient dispersed in a hydrophobic phase comprising a polydimethylsiloxane, Abbott Laboratories, WO2011151418-A2, 2011.
- (7) Hoxmeier, R. J.; Hansen, D. R. Silicone oil gel formulation for use in cosmetic, pharmaceutical products and cable filling applications, comprises block copolymers dissolved in polydimethylsiloxane having specific number average molecular weight, Shell Oil Company, US6160045-A, 2000.
- (8) Clarson, S. J.; Dodgson, K.; Semlyen, J. A. *Polymer* **1985**, *26*, 930.
- (9) Clarson, S. J.; Mark, J. E.; Dodgson, K. *Polymer Communications* **1988**, *29*, 208.
- (10) Bellas, V.; Iatrou, H.; Hadjichristidis, N. *Macromolecules* **2000**, *33*, 6993.
- (11) Smith, S. D.; DeSimone, J. M.; Huang, H.; York, G.; Dwight, D. W.; Wilkes, G. L.; McGrath, J. E. *Macromolecules* **1992**, *25*, 2575.
- (12) Yu, J.; Teyssié, D.; Khalifa, R.; Boileau, S. *Polymer Bulletin* **1994**, *32*, 35.
- (13) Zilliox, J. G.; Roovers, J. E. L.; Bywater, S. *Macromolecules* **1975**, *8*, 573.
- (14) Abbasi, F.; Mirzadeh, H.; Katbab, A.-A. *Polymer International* **2001**, *50*, 1279.
- (15) Li, G.; Yates, M. Z.; Johnston, K. P.; Howdle, S. M. *Macromolecules* **2000**, *33*, 4008.
- (16) Shiho, H.; DeSimone, J. M. *Journal of Polymer Science Part A: Polymer Chemistry* **2000**, *38*, 1139.
- (17) Klein, S.; Manoharan, V.; Pine, D.; Lange, F. *Colloid & Polymer Sci* **2003**, *282*, 7.
- (18) Pelton, R.; Osterroth, A.; Brook, M. A. *Journal of Colloid and Interface Science* **1991**, *147*, 523.
- (19) Richez, A. P.; Farrand, L.; Goulding, M.; Wilson, J. H.; Lawson, S.; Biggs, S.; Cayre, O. J. *Langmuir* **2014**, *30*, 1220.
- (20) Richez, A. P.; Yow, H. N.; Biggs, S.; Cayre, O. J. *Progress in Polymer Science* **2013**, *38*, 897.
- (21) Dawkins, J. V.; Taylor, G. *Polymer* **1979**, *20*, 599.
- (22) Malhotra, S. L.; Bluhm, T. L.; Deslandes, Y. *European Polymer Journal* **1986**, *22*, 391.
- (23) de Paz Báñez, M. V.; Robinson, K. L.; Armes, S. P. *Macromolecules* **1999**, *33*, 451.
- (24) Biggs, S.; Vincent, B. *Colloid & Polymer Sci* **1992**, *270*, 505.
- (25) Xia, Y.; Whitesides, G. M. *Annual Review of Materials Science* **1998**, *28*, 153.
- (26) Park, M.; Harrison, C.; Chaikin, P. M.; Register, R. A.; Adamson, D. H. *Science* **1997**, *276*, 1401.
- (27) Son, J. G.; Gotrik, K. W.; Ross, C. A. *ACS Macro Letters* **2012**, *1*, 1279.
- (28) Lo, T.-Y.; Chao, C.-C.; Ho, R.-M.; Georgopoulos, P.; Avgeropoulos, A.; Thomas, E. L. *Macromolecules* **2013**, *46*, 7513.

- (29) Langowska, K.; Palivan, C. G.; Meier, W. *Chemical Communications* **2013**, *49*, 128.
- (30) Car, A.; Baumann, P.; Duskey, J. T.; Cham, M.; Bruns, N.; Meier, W. *Biomacromolecules* **2014**, *15*, 3235.
- (31) Spulber, M.; Baumann, P.; Saxer, S. S.; Pieleles, U.; Meier, W.; Bruns, N. *Biomacromolecules* **2014**, *15*, 1469.
- (32) Gomez, L. R.; Vega, D. A.; Ninago, M.; Ciolino, A. E.; Villar, M. A.; Valles, E. M. *Polymer* **2015**, *59*, 180.
- (33) Jeong, J. W.; Park, W. I.; Kim, M.-J.; Ross, C. A.; Jung, Y. S. *Nano Letters* **2011**, *11*, 4095.
- (34) Son, J. G.; Chang, J.-B.; Berggren, K. K.; Ross, C. A. *Nano Letters* **2011**, *11*, 5079.
- (35) Park, S.-M.; Liang, X.; Harteneck, B. D.; Pick, T. E.; Hiroshiba, N.; Wu, Y.; Helms, B. A.; Olynick, D. L. *Acs Nano* **2011**, *5*, 8523.
- (36) Iyama, K.; Nose, T. *Polymer* **1998**, *39*, 651.
- (37) Nunns, A.; Whittell, G. R.; Winnik, M. A.; Manners, I. *Macromolecules* **2014**, *47*, 8420.
- (38) Ruez, J.; Manners, I.; Winnik, M. A. *Journal of the American Chemical Society* **2002**, *124*, 10381.
- (39) Patten, T. E.; Matyjaszewski, K. *Advanced Materials* **1998**, *10*, 901.
- (40) Matyjaszewski, K. *Macromolecules* **2012**, *45*, 4015.
- (41) Moad, G.; Mayadunne, R. T. A.; Rizzardo, E.; Skidmore, M.; Thang, S. H. *Macromolecular Symposia* **2003**, *192*, 1.
- (42) Chiefari, J.; Chong, Y. K.; Ercole, F.; Krstina, J.; Jeffery, J.; Le, T. P. T.; Mayadunne, R. T. A.; Meijs, G. F.; Moad, C. L.; Moad, G.; Rizzardo, E.; Thang, S. H. *Macromolecules* **1998**, *31*, 5559.
- (43) Zetterlund, P. B.; Kagawa, Y.; Okubo, M. *Chemical Reviews* **2008**, *108*, 3747.
- (44) Huan, K.; Bes, L.; Haddleton, D. M.; Khoshdel, E. *Journal of Polymer Science Part A: Polymer Chemistry* **2001**, *39*, 1833.
- (45) Zhao, W.; Fonsny, P.; FitzGerald, P.; Warr, G. G.; Perrier, S. *Polymer Chemistry* **2013**, *4*, 2140.
- (46) Fielding, L. A.; Derry, M. J.; Ladmiral, V.; Rosselgong, J.; Rodrigues, A. M.; Ratcliffe, L. P. D.; Sugihara, S.; Armes, S. P. *Chemical Science* **2013**, *4*, 2081.
- (47) Boisse, S.; Rieger, J.; Belal, K.; Di-Cicco, A.; Beaunier, P.; Li, M.-H.; Charleux, B. *Chemical Communications* **2010**, *46*, 1950.
- (48) Sugihara, S.; Blanazs, A.; Armes, S. P.; Ryan, A. J.; Lewis, A. L. *Journal of the American Chemical Society* **2011**, *133*, 15707.
- (49) Chambon, P.; Blanazs, A.; Battaglia, G.; Armes, S. P. *Langmuir* **2011**, *28*, 1196.
- (50) Blanazs, A.; Warren, N. J.; Lewis, A. L.; Armes, S. P.; Ryan, A. J. *Soft Matter* **2011**, *7*, 6399.
- (51) Rieger, J.; Grazon, C.; Charleux, B.; Alaimo, D.; Jérôme, C. *Journal of Polymer Science Part A: Polymer Chemistry* **2009**, *47*, 2373.
- (52) Zhang, X.; Boisse, S.; Bui, C.; Albouy, P.-A.; Brulet, A.; Li, M.-H.; Rieger, J.; Charleux, B. *Soft Matter* **2012**, *8*, 1130.
- (53) Zhang, X.; Rieger, J.; Charleux, B. *Polymer Chemistry* **2012**, *3*, 1502.
- (54) Semsarilar, M.; Jones, E. R.; Blanazs, A.; Armes, S. P. *Advanced Materials* **2012**, *24*, 3378.
- (55) Wan, W.-M.; Sun, X.-L.; Pan, C.-Y. *Macromolecular Rapid Communications* **2010**, *31*, 399.
- (56) Cai, W.; Wan, W.; Hong, C.; Huang, C.; Pan, C. *Soft Matter* **2010**, *6*, 5554.
- (57) Semsarilar, M.; Ladmiral, V.; Blanazs, A.; Armes, S. P. *Polymer Chemistry* **2014**, *5*, 3466.
- (58) Lim, K. T.; Lee, M. Y.; Hwang, H. S.; Heo, H.; Hong, S.-S.; Park, J. M. *Polymer Bulletin* **2001**, *47*, 135.

- (59) Fielding, L. A.; Lane, J. A.; Derry, M. J.; Mykhaylyk, O. O.; Armes, S. P. *Journal of the American Chemical Society* **2014**, *136*, 5790.
- (60) Charleux, B.; Delaittre, G.; Rieger, J.; D'Agosto, F. *Macromolecules* **2012**, *45*, 6753.
- (61) Chambon, P.; Blanazs, A.; Battaglia, G.; Armes, S. P. *Macromolecules (Washington, DC, U. S.)* **2012**, *45*, 5081.
- (62) Li, Y.; Armes, S. P. *Angewandte Chemie International Edition* **2010**, *49*, 4042.
- (63) Houillot, L.; Bui, C.; Farcet, C.; Moire, C.; Raust, J.-A.; Pasch, H.; Save, M.; Charleux, B. *ACS Applied Materials & Interfaces* **2010**, *2*, 434.
- (64) Houillot, L.; Bui, C.; Save, M.; Charleux, B.; Farcet, C.; Moire, C.; Raust, J.-A.; Rodriguez, I. *Macromolecules* **2007**, *40*, 6500.
- (65) Pei, Y.; Sugita, O. R.; Thurairajah, L.; Lowe, A. B. *RSC Advances* **2015**, *5*, 17636.
- (66) Semsarilar, M.; Ladmiral, V.; Blanazs, A.; Armes, S. P. *Langmuir* **2012**, *29*, 7416.
- (67) Trent, J. S. *Macromolecules* **1984**, *17*, 2930.
- (68) Ilavsky, J.; Jemian, P. R. *Journal of Applied Crystallography* **2009**, *42*, 347.
- (69) Zhang, F.; Ilavsky, J.; Long, G.; Quintana, J. G.; Allen, A.; Jemian, P. *Metall and Mat Trans A* **2010**, *41*, 1151.
- (70) Zehm, D.; Ratcliffe, L. P. D.; Armes, S. P. *Macromolecules* **2012**, *46*, 128.
- (71) Ratcliffe, L. P. D.; Ryan, A. J.; Armes, S. P. *Macromolecules* **2013**, *46*, 769.
- (72) Jones, E. R.; Semsarilar, M.; Blanazs, A.; Armes, S. P. *Macromolecules* **2012**, *45*, 5091.
- (73) Warren, N. J.; Armes, S. P. *Journal of the American Chemical Society* **2014**, *136*, 10174.
- (74) Zhang, X.; Boissé, S. p.; Zhang, W.; Beaunier, P.; D'Agosto, F.; Rieger, J.; Charleux, B. *Macromolecules* **2011**, *44*, 4149.
- (75) Wan, W.-M.; Sun, X.-L.; Pan, C.-Y. *Macromolecules* **2009**, *42*, 4950.
- (76) Blanazs, A.; Ryan, A. J.; Armes, S. P. *Macromolecules* **2012**, *45*, 5099.
- (77) Warren, N. J.; Mykhaylyk, O. O.; Mahmood, D.; Ryan, A. J.; Armes, S. P. *J Am Chem Soc* **2014**, *136*, 1023.
- (78) Westheimer, F. *Science* **1987**, *235*, 1173.
- (79) Wadley, M. L.; Cavicchi, K. A. *Journal of Applied Polymer Science* **2010**, *115*, 635.
- (80) Skrabania, K.; Miasnikova, A.; Bivigou-Koumba, A. M.; Zehm, D.; Laschewsky, A. *Polymer Chemistry* **2011**, *2*, 2074.
- (81) Moad, G.; Rizzardo, E.; Thang, S. H. *Accounts of Chemical Research* **2008**, *41*, 1133.
- (82) Blanazs, A.; Madsen, J.; Battaglia, G.; Ryan, A. J.; Armes, S. P. *Journal of the American Chemical Society* **2011**, *133*, 16581.
- (83) Flory, P. J. *Journal of the American Chemical Society* **1940**, *62*, 1561.
- (84) Glatter, O.; Kratky, O. *Small-angle X-ray Scattering*; Academic Press: London, 1982.
- (85) Pedersen, J. S.; Gerstenberg, M. C. *Macromolecules* **1996**, *29*, 1363.
- (86) Pedersen, J. S. *Journal of Chemical Physics* **2001**, *114*, 2839.
- (87) Semsarilar, M.; Penfold, N. J. W.; Jones, E. R.; Armes, S. P. *Polymer Chemistry* **2015**.
- (88) Derry, M. J.; Fielding, L. A.; Armes, S. P. *Polymer Chemistry* **2015**.
- (89) Warren, N. J.; Mykhaylyk, O. O.; Ryan, A. J.; Williams, M.; Doussineau, T.; Dugourd, P.; Antoine, R.; Portale, G.; Armes, S. P. *Journal of the American Chemical Society* **2014**.
- (90) Verber, R.; Blanazs, A.; Armes, S. P. *Soft Matter* **2012**, *8*, 9915.